Commun. Comput. Phys.
doi: 10.4208/cicp.060515.161115b

Vol. **20**, No. 2, pp. 325-352
August 2016

On the Spurious Mode Generation Induced by Spectral-Like Optimized Interpolation Schemes Used in Computational Acoustics

Guilherme Cunha[1] and Stéphane Redonnet[2,*]

[1] *Department of Numerical Fluid Mechanics, Onera – French Aerospace Lab, F-92322 Châtillon, France.*

[2] *Department of Aeroacoustics, Onera – French Aerospace Lab, F-92322 Châtillon, France.*

Received 6 May 2015; Accepted (in revised version) 16 November 2015

Abstract. The present work constitutes a fraction of a more extensive study that is devoted to numerical methods in acoustics. More precisely, we address here the interpolation process, which is more and more frequently used in Computational Acoustics – whether it is for enabling multi-stage hybrid calculations, or for easing the proper handling of complex configurations via advanced techniques such as Chimera grids or Immersed Boundary Conditions. In that regard, we focus on high-order interpolation schemes, so as to analyze their intrinsic features and to assess their effective accuracy. Taking advantage of specific insights that had been previously achieved by the present authors regarding standard high-order interpolation schemes (of centered nature), we here focus on their so-called *spectral-like optimized* counterparts (of both centered and noncentered nature). The latter spectral-like optimized schemes are analyzed thoroughly thanks to dedicated theoretical developments, which allow highlighting better what their strengths and weaknesses are. Among others, the various ways such interpolation schemes can degrade acoustic signals they are applied to are carefully investigated from a theoretical point-of-view. Besides that, specific criteria that could help in optimizing interpolation schemes better are provided, along with generic rules about how to minimize the signal degradation induced by existing interpolation schemes, in practice.

AMS subject classifications: 65D05, 76M25, 41A05

Key words: Noncentered interpolation, centered interpolation, high-order, spectral-like optimization, spurious modes generation, computational acoustics.

*Corresponding author. *Email address:* stephane.redonnet@onera.fr (S. Redonnet)

 ©2016 Global-Science Press

https://doi.org/10.4208/cicp.060515.161115b Published online by Cambridge University Press

1 Introduction

Nowadays, many fields of research focus on the modeling of noise phenomena, which finds plenty of applications within numerous domains. Indeed, adequately modeling and predicting noise phenomena can help improving existing technologies, such as reducing the noise annoyances by industrial products (e.g. aircraft, trains or cars, wind turbines, computers). It can also help optimizing specific acoustic-based devices, such as those used for non destructive control, non intrusive medical imaging, seismic monitoring, and so on. Finally, it can facilitate the emergence of new technologies, e.g. alternative and innovative acoustic-based devices (e.g. sensorless tactile screens, ultra-sound medical curative techniques). On another hand, since acoustics is a complex discipline, researchers are now bounded to make an intensive use of numerical simulation, which constitutes a powerful means of investigations, when coming in complement to the experimentation.

This, however, requires the continuous development and improvement of modeling and solving techniques that can account for all mechanisms underlying the noise generation and/or propagation phenomena. Indeed, noise finds its origin in numerous source mechanisms such as structural vibrations, fluid motions, flow interactions with structures, gas combustion or explosions. Once they have been generated by these sources, acoustic waves propagate within the surrounding environment, which is generally constituted with one or several media of various complexity (e.g. comprising solid bodies and/or medium heterogeneity). During such propagation phase, acoustic waves may thus be submitted to numerous and important alterations in terms of amplitude, phase or frequency, which all result from mechanisms as diverse as reflection and diffraction effects by solid structures, convection by fluid motions, refraction and diffusion by the medium heterogeneity (e.g. turbulence, temperature gradients), absorption by the medium viscosity, etc.

Many of the acoustic generation processes and most of the acoustic propagation mechanisms are relevant to the physics of fluid dynamics, and can thus be simulated by numerically solving the Navier-Stokes equations. However, the specificity of acoustic phenomena implies that such solving is achieved following very precise strategies. In particular, this is what led to the emergence of Computational AeroAcoustics (CAA), a scientific discipline that rapidly progressed over the past twenty years. Among others, such discipline promoted the development of highly-accurate numerical schemes, whose minimal dissipation and dispersion properties are mandatory for acoustic waves are correctly simulated over long propagation distances and time durations [1]. As an illustration, given their higher accuracy and, thus, ability to simulate wave-like phenomena on coarser grids [2], high-order Finite-Difference (FD) methods have emerged as a valuable alternative to more traditional low-order methods that are usually employed in other disciplines (e.g. Computational Fluid Dynamics, CFD).

At the present time, however, and despite of the continuous development of computational tools and resources, it is still very challenging to simulate aero-acoustic problems

https://doi.org/10.4208/cicp.060515.161115b Published online by Cambridge University Press

following a direct manner, i.e. via a single calculation. As an example, except in particular situations, e.g. academic configurations, it is nearly impossible to compute simultaneously both the acoustic generation and propagation phenomena, which underlying mechanisms generally differ by their intrinsic characteristics, such as energy and length scales of phenomena involved.

Therefore, in most practical cases, aeroacoustic problems are solved following a hybrid manner [3–7], according which the overall problem is partitioned into several sub-problems, the latter being numerically simulated using the most adapted strategy, that is, the one offering the best trade-off between accuracy and CPU cost.

Such a hybrid scenario however implies that the various sub-problems are linked (or coupled) altogether, which generally requires that a data transfer is achieved between them. Needless to say, such a data transfer between two stages of a hybrid method must be conducted in a conservative fashion, that is, without leading to information loss or duplication. In particular, and because of the mismatches between the discrete formulations associated with all stages, such a data transfer generally relies on space and/or time interpolation techniques.

On another hand, and from a more global perspective, it appears that interpolation techniques are more and more extensively used for solving practical acoustic problems, whether the latter are addressed following a direct or a hybrid approach. As an example, for practical applications involving complex geometries that cannot be easily handled via a single body-fitted mesh, use is often made of Chimera techniques, which rely on elementary overset-grids that overlap each other, and that are linked altogether via interpolations [2,3,8]. In addition, many advanced computational techniques now used within an aeroacoustic context (e.g. multi-size-mesh/multi-time-step techniques [9], immersed boundary methods [10,11]) also rely on space and/or time interpolation processes. At this point, it is clear that, for not jeopardizing the aeroacoustic calculations they are part of, all interpolation operations must preserve the accuracy of data, at least as much as the numerical schemes used do.

On that stage, one can recall that literature abounds in studies that focused on interpolation techniques, wheter the latter are of low or high order-of-accuracy. In particular, some of these works [2,10,12,13] highlighted a major side-effect of the interpolation process, which is the so-called signal degradation such process may induce onto that part of the interpolated data whose frequency (in terms of wavenumber) is high. With the view of minimizing such a side-effect, some authors thus proposed innovative interpolation schemes that, being of either centered [2,10] or noncentered [10,12] nature, are optimized in a spectral-like sense, that is, in the wavenumber space.

The point is that, as first demonstrated in [13], when interpolated, a signal may not solely be subjected to a degradation of its higher frequency contents, but it can also suffer from additional alterations, to occur over the whole spectrum, because of the so-called *spuriousing* and subsequent *aliasing* phenomena. Since none of the referred studies had provided a thorough analysis of these two specific side-effects, one could legitimately wonder how spectral-like optimized interpolation schemes might effectively be-

https://doi.org/10.4208/cicp.060515.161115b Published online by Cambridge University Press

have when subjected to them.

Recently, the present authors have proposed an original formalism [14] that unifies all elements needed for understanding the signal degradation induced by interpolation, thus allowing to characterize both the spuriousing and the aliasing phenomena, as well as to predict their impact in terms of signal degradation. Additionally, such formalism made it possible to assess better standard high-order interpolation schemes of centered nature [14]. It appeared thus natural to now also access standard noncentered and spectral-like optimized schemes, the latter being either of centered [2, 10] or noncentered [10, 12] nature. This is what motivated the present study, and constitutes the subject of the present article.

2 Interpolation schemes

As was said above, the present work relies on a dedicated formalism [14] that was specifically developed by the present authors for studying interpolation techniques. Such formalism, which is briefly recalled in Appendix A, relies on the theoretical study of $1D$ explicit interpolations operating on uniformly discretized donor grids. This choice can be justified by the following reasons:

1. Any multidimensional interpolation can be written as a tensorization of mono-dimensional ones [15].
2. In multidimensional problems, implicit (compact) interpolation methods do not present enough trade-offs, if one compares the complexity of their implementation with respect to the accuracy gain they effectively offer [2].
3. Interpolations are generally achieved in the computational domain (Cartesian grid) rather than in the physical one (curvilinear grid) [16].

Let us then consider a given one-dimensional interpolation stencil built from uniformly spaced points, such as the one depicted in Fig. 1. Here, x indicates any position included in the interval $[x_n, x_{n+1}[$ to be covered by the interpolation stencil, whose first and last points are indexed by $J_{\min}$ and $J_{\max}$ (both included in $\mathbb{Z}$) respectively.

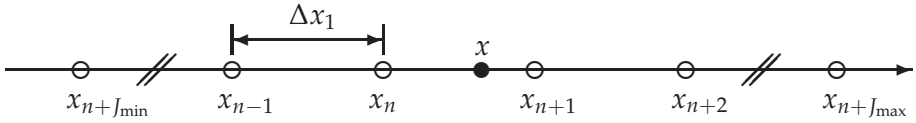


Figure 1: A given receiver point, x, and its associated $|J_{\max}|+|J_{\min}|+1$ donor points, positioned along a one-dimensional interpolation stencil.

Without a loss of generality, we can assume that the stencil nodes correspond to a set of donor points associated with a uniform grid to be defined as $x_n = n\Delta x_1$, with $n \in \mathbb{Z}$ and Δx_1 the discretization step. Analogously, x can be seen as an interpolation point

https://doi.org/10.4208/cicp.060515.161115b Published online by Cambridge University Press

associated with a given receiver grid, the latter being defined such that $x = m\Delta x_2 + d$, with $m \in \mathbb{Z}$ and $d \in [-\Delta x_1/2, \Delta x_1/2[$ [†]. For any continuous function, $f : \mathbb{R} \longrightarrow \mathbb{R}$, its corresponding interpolated function can then be written as:

$$\mathcal{I}[f](x) = \sum_{n=-\infty}^{+\infty} \mathbf{1}_{[0,1[}\left(\frac{x}{\Delta x_1} - n\right) \sum_{j=J_{\min}}^{J_{\max}} S_j\left(\frac{x}{\Delta x_1} - n\right) f((n+j)\Delta x_1), \tag{2.1}$$

where $\mathbf{1}_{[0,1[}(\cdot)$ is the identity function,

$$\mathbf{1}_{[0,1[}(x) = \begin{cases} 1, & \text{if } x \in [0,1[, \\ 0, & \text{if } x \notin [0,1[. \end{cases} \tag{2.2}$$

and S_j are the interpolation schemes coefficients, whose respective values are still to be evaluated.

At this stage, one can first underline that, for avoiding Eq. (2.1) to turn into the extrapolation operator, it is here imposed that $[x_n, x_{n+1}[$ is included in $[x_{n+J_{\min}}, x_{n+J_{\max}}[$. One can also notice that the particular case of a centered interpolation scheme is met when $[x_n, x_{n+1}[$ corresponds to the central interval included in $[x_{n+J_{\min}}, x_{n+J_{\max}}[$. Otherwise, the interpolation operator is of noncentered kind. Finally, in the present work, only one type of 'standard' interpolation will be considered, that is, the Lagrange one. As a reminder, let us precise that a $(|J_{\max}|+|J_{\min}|+1)th$-order Lagrange interpolation is obtained by setting $S_j(\cdot) = P_j(\cdot)$, $\forall j \in \{J_{\min}, \cdots, 0, 1, \cdots, J_{\max}\}$, with

$$P_j(x) = \Pi_{p=J_{\min}, p\neq j}^{J_{\max}} \frac{x-p}{j-p}. \tag{2.3}$$

3 Interpolation process and signal degradation – brief reminder

As stated earlier, for performing aeroacoustic calculations one generally needs to make use of highly accurate methods. As a corollary, their highly accurate character must not be jeopardized by the interpolation processes these methods may partly rely on. This implies that the interpolation techniques to be employed are such that, once applied to a given aeroacoustic signal, they will degrade it in a very minimal way. Now, as was also recalled earlier, a previous work by the present authors [14] showed how the signal degradation by a given interpolation operator may be efficiently characterized and analyzed, provided that the interpolation process is sketched as a composition of three successive steps:

0. the discretization of the signal associated continuous function, $f(\cdot)$, onto a so-called *donor* grid, resulting in a discretized function, $f_d(\cdot)$,

[†]In the forthcoming sections, the subscript $i \in \{1,2\}$ associated with a given variable indicates on which grid such variable is considered, that is, donor, $i=1$, or receiver, $i=2$. Additionally, unless stated otherwise, $d=0$ (see Appendix *B*).

https://doi.org/10.4208/cicp.060515.161115b Published online by Cambridge University Press

1. the reconstruction of a continuous function approximating $f(\cdot)$, with the help of an interpolation operator, $\mathcal{I}[f_d](\cdot)$, and

2. the projection of the reconstructed function, $\mathcal{I}[f_d](\cdot)$, onto a so-called *receiver* grid.

In the following, the expression *interpolation process* indicates the composition of the three previous steps. On another hand, the term *interpolation* solely refers to step #1, that is, the operation that reconstructs the discrete function $f_d(\cdot)$ into an approximated *continuous* function $\mathcal{I}[f_d](\cdot)$. When considering the sole step #1, it can be shown [14] that its associated *interpolation* operation alters the original signal associated continuous function, $f(\cdot)$, following two mechanisms:

1. The degradation of correct information, through the alteration of that part of the signal which falls in the higher part of spectrum (in terms of wavenumbers).

2. The creation of incorrect information, through the generation of spurious contents (or modes), which are also of high wavenumber.

One can thus conclude that the interpolated (continuous) signal, $\mathcal{I}[f_d](\cdot)$, will be accurate only over the low- and mid-frequency ranges (in terms of wavenumbers). However, it can be shown [14] that, once projected onto a given receiver grid (step #2), such signal may be subjected to another side-effect, depending on the ratio between the donor and the receiver respective discretizations; indeed, any of the signal components that is to be under-resolved on the receiver grid will then be aliased back into the low- and mid-level frequency ranges. Therefore, at the end, once it will have been successively (i) discretized onto a donor grid, (ii) interpolated from the latter, and then (iii) projected onto a receiver one, a given aeroacoustic signal may end up being entirely degraded, that is, altered *over its whole spectrum*. In particular, such degradation of the signal will closely depend on the total amount of spurious modes that will have been incorrectly generated, and then further aliased. In other words, the signal degradation to be induced by a given interpolation process may be strongly driven by both the spuriousing (or spurious mode generation) and the subsequent aliasing phenomena it is characterized by.

4 Spectral-like optimization of interpolation schemes

With the view of preventing at best aeroacoustic signals to be degraded by interpolation, some authors have proposed innovative interpolation schemes (either of centered [2, 10] or noncentered [10, 12] nature), which were optimized following a spectral-like strategy, that is to say, in the wavenumber space. Indeed, such so-called *spectral-like* optimization approach aims at enhancing the scheme's ability to preserve the acoustic dispersion/dissipation properties of interpolation schemes, by minimizing the error they may induce on the spectral components of any given harmonic signal.

https://doi.org/10.4208/cicp.060515.161115b Published online by Cambridge University Press

4.1 Spectral-like optimization of centered interpolation schemes

In order to optimize centered interpolation schemes following a spectral-like strategy, one can refer to works by Tam and Kurbatskii [10].

4.1.1 Spectral-like optimization of centered interpolation schemes: principle

The spectral-like optimization proposed in [10] consists in a minimization of the integrated error that is to be made by the interpolation scheme on a single Fourier component of the form $f(x)=e^{i\alpha x}$:

$$E(x)=\int_0^{\kappa}\left|e^{i\alpha x}-\mathcal{I}[e^{i\alpha x}]\right|^2 d(\alpha\Delta x_1). \tag{4.1}$$

In the above, κ indicates the optimization parameter, which determines the frequency range interval over which minimizing the integrated error, with that interval covered by all wavenumbers α. Now, by making use of Eq. (2.1), one can explicitly express the integrated error associated with the considered scheme:

$$E(x)=\int_0^{\kappa}\left|e^{i\alpha\eta\Delta x_1}-\sum_{j=J_{\min}}^{J_{\max}}S_j(\eta)e^{i\alpha j\Delta x_1}\right|^2 d(\alpha\Delta x_1), \tag{4.2}$$

where $\eta=x/\Delta x_1-n$ and $x\in[n\Delta x_1,(n+1)\Delta x_1[$, implying $\eta\in[0,1[$. Based on that, one can then identify which set of interpolation coefficients (S_j) is the optimal one, that is, the one that will ensure a minimal integrated error.

In addition to such requirement for a minimal integrated error, the interpolation operator coefficients (S_j) are also imposed a specific constraint, so that no error is made on the zero-wavenumber component:

$$\left|1-\sum_{j=J_{\min}}^{J_{\max}}S_j(\eta)\right|=0,\quad\forall\eta\in[0,1[. \tag{4.3}$$

4.1.2 Spectral-like optimization of centered interpolation schemes: effective efficiency

In [10], various centered interpolation schemes were spectral-like optimized following the procedure described above. All associated sets of interpolation coefficients $S_j(\cdot)$ were determined by considering $\kappa=1.0$, before the various spectral-like schemes were compared against their standard (i.e. non-optimized) counterparts. Based on the observations made, the relevance of the spectral-like optimization process was then discussed by the authors, their main conclusion being that, regarding centered interpolations, spectral-like optimized schemes exhibit slightly better properties than their standard counterpart.

One can here point out the fact that the referred study did not really address the question of the spurious mode generation, nor of its possible impact on the spectral-like optimization procedure. Indeed, on that stage, the authors simply mentioned that, from

https://doi.org/10.4208/cicp.060515.161115b Published online by Cambridge University Press

the moment the interpolated signal would be used within a LES or a CAA computation, all of its high frequency (and, thus, possibly spurioused) contents would likely be filtered out during the calculation, thanks to the selective artificial damping or filtering procedures these numerical methods usually employ.

The point is that, as was discussed above and demonstrated in [14], long before it can be filtered out by such procedures, and because of its interpolation and further projection onto the (receiver) grid over which the calculation is conducted, any of the high frequency components may partly be degenerated into spurious and aliased modes that will then pollute *the whole spectrum* [13, 14, 17]. In this case, *none* of the spurious contents lying within the low- and mid-parts of the spectrum will be suppressed by artificial selective damping or filtering techniques.

As an illustration, let us consider a signal composed of several test functions $f_k(\cdot)$, to be allotted an identical amplitude along with various wavenumbers k

$$f_k(x)=\cos\left(\frac{k\pi}{16\Delta x_1}x\right)\exp\left(-\left(\frac{x}{16\Delta x_1}\right)^2\right),\quad k\in[0,14]. \tag{4.4}$$

Fig. 2 depicts the signal's spectrum, as obtained by analytically evaluating and adding all functions $f_k(\cdot)$ Fourier transforms.

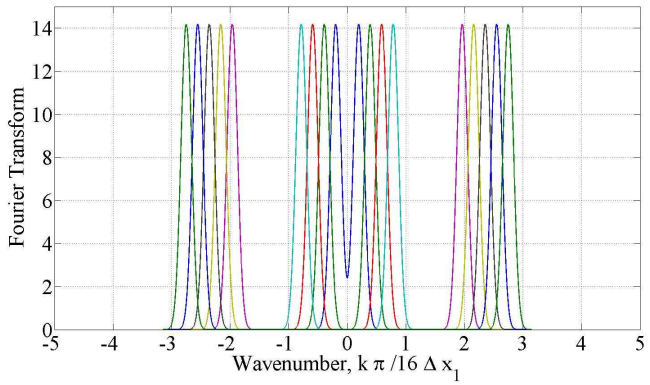
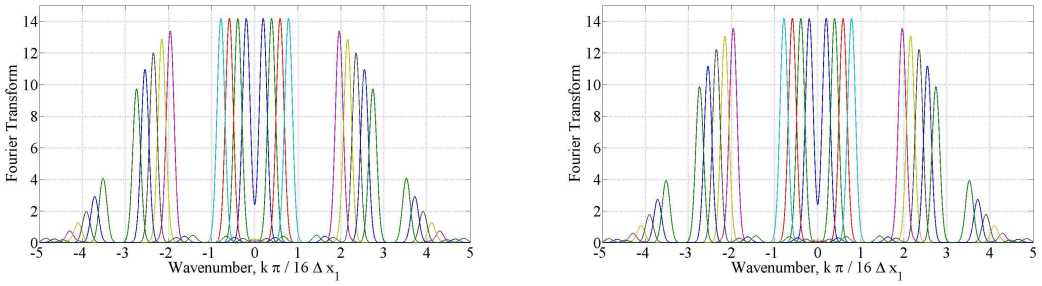


Figure 2: Spectrum of a signal composed with a set of $f_k(\cdot)$ functions associated with various $k\in[0,14]$ (see Eq. (4.4)).

Let us now interpolate the previous signal from a uniform $1D$ donor grid of discretization step $\Delta x_1=1$ towards a receiver grid associated with a uniform $1D$ grid of discretization step $\Delta x_2=(3/5)\times\Delta x_1$. For doing so, let us submit such signal to a 7-point stencil interpolation operator, with the latter being centered on each receiver point (i.e. $J_{\min}=-3$ and $J_{\max}=3$) so that the interpolation configuration is identical to the one assessed in reference [10]. Fig. 3 compares the spectra of the resulting interpolated signal, as obtained via either the standard (Fig. 3(a)) or the spectral-like optimized (Fig. 3(b)) version of such centered 7-point interpolation operator.

https://doi.org/10.4208/cicp.060515.161115b Published online by Cambridge University Press



(a) (b)

Figure 3: Spectrum of the interpolated signal composed with functions $f_k(\cdot)$, as obtained through a centered 7-point interpolation scheme of either (a) standard or (b) spectral-like optimized [10] types. In the present case, $\Delta x_2 = (3/5) \times \Delta x_1$, with $\Delta x_1 = 1$.

As can be seen, whether the interpolation operator is of standard or spectral-like optimized kind, it induces the generation of spurious modes *all over the spectrum*. Concerning more particularly the standard operator, one can observe that the lower part of the spectrum is polluted with spurious modes whose amplitude rise up to 3.3% of the original (that is, non-spurioused) signal content. Concerning now the spectral-like optimized operator, the situation is roughly similar, with a pollution of the lower part of the spectrum by spurious modes whose amplitude rise up to 3.0% of the original content. This clearly shows that, when it comes to minimize the spurious modes generation (and subsequent aliasing), a spectral-like optimization of interpolation schemes may not be of great help.

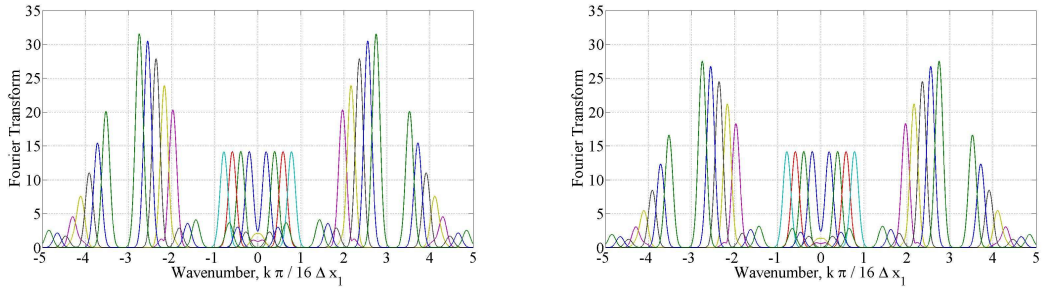
On that stage, one can point out that, although these 3% amplitude levels of spurious modes may appear to be small, they are of relative nature. Indeed, the absolute error level resulting from the spuriousing mechanism of any interpolation scheme is to be driven by the magnitude of the original signal's high frequency contents. Now, if one considers how energetic some typical high-frequency aeroacoustic occurrences (such as aerodynamic ones, e.g. vortices) may be [1, 6], one can legitimately wonder about the effective accuracy of interpolation schemes, when used for solving practical problems involving other components than purely acoustic ones – which is likely to occur in many situations, as, for instance, aerodynamic noise issues [1, 6–8].

4.2 Spectral-Like optimization of noncentered interpolation schemes

4.2.1 Spectral-like optimization of non centered interpolation schemes – principle and effective efficiency

Following the same approach by Tam and Kurbatskii [10], one can also optimize noncentered interpolation operators in a spectral-like sense, by making use of the same Eq. (4.2) and of its associated constraint of Eq. (4.3). Now, let us repeat the interpolation exercise conducted in the previous section but, this time, with a noncentered operator of same

https://doi.org/10.4208/cicp.060515.161115b Published online by Cambridge University Press



(a) (b)

Figure 4: Spectrum of the interpolated signal composed with functions $f_k(\cdot)$, as obtained through a noncentered 7-point interpolation scheme of either (a) a standard or (b) a spectral-like optimized [10] types. In the present case, $\Delta x_2 = (3/5)\times\Delta x_1$, with $\Delta x_1 = 1$.

stencil size (7 points) to be defined such that $J_{\min} = -5$ and $J_{\max} = 1$, that is, with the receiver point located at the donor grid's first interval. As previously done for its centered counterpart, Fig. 4 compares the spectra of the resulting interpolated signal, as obtained via either the standard (Fig. 4(a)) or the spectral-like optimized (Fig. 4(b)) version of such noncentered 7-point interpolation operator.

As can be noticed, for both cases, the spurious modes are more important than the ones resulting from a centered interpolation (see Fig. 3). Indeed, over the lower part of the spectrum, the amplitude of the spurious modes generated by such a noncentered standard (resp. spectral-like optimized) interpolation scheme now reaches up to 29.0% (resp. 22.3%) of the original signal's content. In addition, regarding now the upper part of the spectrum, these noncentered interpolators both lead to a strong amplification rate (of almost 100%). This indeed was to be expected since noncentered interpolation schemes are known to be strong amplifiers of high-wavenumber contents [10, 12].

4.2.2 Amplification controlled spectral-like optimization of noncentered interpolation schemes – principle and effective efficiency

With the view of remedying such issue, recently, spectral-like optimized interpolation schemes with amplification control have been proposed [12]. The latter schemes are based on an improved version of the optimization approach, following which the interpolation scheme coefficients are still obtained through a minimization of the integrated interpolation error to be made on a single Fourier component of the form $f(x) = e^{i\alpha x}$, but with such error being now defined in a *relative* sense:

$$E(x) = \int_0^{\kappa} \left| 1 - \frac{\mathcal{I}[e^{i\alpha x}]}{e^{i\alpha x}} \right|^2 d(\alpha\Delta x_1) = \int_0^{\kappa} \left| 1 - \sum_{j=J_{\min}}^{J_{\max}} S_j(\eta) e^{i\alpha(j-\eta)\Delta x_1} \right|^2 d(\alpha\Delta x_1). \tag{4.5}$$

Additional constraints are also imposed, so that the resulting scheme is *Pth*-order

https://doi.org/10.4208/cicp.060515.161115b Published online by Cambridge University Press

accurate:

$$\left|\delta_0^r - \sum_{j=J_{\min}}^{J_{\max}} S_j(\eta)(j+\eta)^r\right| = 0, \quad \forall \eta \in [0,1[\quad \text{and} \quad \forall r \in \{0,1,2,\cdots,P-1\}. \tag{4.6}$$

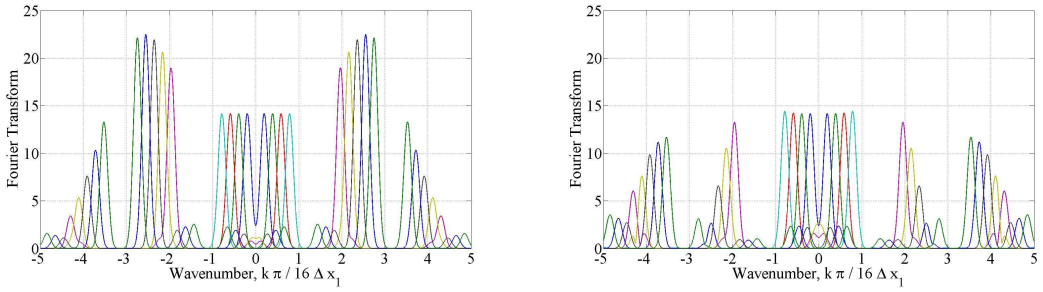
Finally, constituting the key idea of such improved optimization technique, a last constraint is applied, which aims at controlling the amplification level of high-wavenumber contents:

$$\left|\int_0^\pi \left(\sum_{j=J_{\min}}^{J_{\max}} S_j(\eta) e^{i\alpha(j-\eta)\Delta x_1}\right)^{2q} d(\alpha\Delta x_1) - (1-\beta)^{2q}\right| = 0, \tag{4.7}$$

with q and β two optimization parameters that are to be determined numerically.

As an illustration, let us consider a noncentered interpolation scheme of 6-point stencil such that $J_{\min} = -4$ and $J_{\max} = 1$, that is to say, with the receiver point located at the donor grid's first interval. Let us now optimize such scheme following the spectral-like approach with amplification control, by identifying which coefficients minimize Eq. (4.5), when $\kappa = 2\pi/5$, whereas verifying Eq. (4.6), with $P = 5$.

In order to assess the accuracy of the resulting scheme, let us now apply it to the previous signal (composed with test functions $f_k(\cdot)$ of Eq. (4.4)), and compare the spectrum of the interpolated signal against that of its standard counterpart. As can be seen by comparing Figs. 5(a) and 5(b), the present spectral-like optimized and amplification controlled noncentered scheme does not induce any amplification of the signal's high-wavenumber contents, on the contrary to what happened with its standard counterpart.



(a) (b)

Figure 5: Spectrum of the interpolated signal composed with functions $f_k(\cdot)$, as obtained through a noncentered 6-point interpolation scheme of either (a) standard or (b) spectral-like optimized with amplification control [12] types. In the present case, $\Delta x_2 = (3/5) \times \Delta x_1$, with $\Delta x_1 = 1$.

However, as can also be observed on the same figure, and still with respect to its standard equivalent, the present spectral-like optimized noncentered interpolation generates spurious modes of higher amplitudes over the whole spectrum. More precisely, over the

https://doi.org/10.4208/cicp.060515.161115b Published online by Cambridge University Press

lower part of the signal spectrum, the amplitude ratio between the interpolated (i.e. spurioused) and the original contents reaches 18.0% for the standard interpolation scheme, whereas it rises up to 19.0% for the spectral-like optimized and amplification controlled one. In other words, far from having minimized it, the spectral-like optimization process has here *magnified* the spuriousing mechanism associated with the present noncentered 6-point interpolation scheme.

5 Theoretical study of the signal degradation induced by spectral-like optimized interpolation schemes

All what precedes clearly shows that, whether they are of centered or noncentered nature, spectral-like optimized interpolation schemes suffer as much as standard ones from the spuriousing phenomenon. More importantly, in some situations, the latter phenomena may even be magnified by the spectral-like optimization procedure.

With the view of investigating that point further, the present section details a specific analysis that was achieved in order to characterize the signal degradation induced by spectral-like optimized schemes (whether the latter are of centered or noncentered natures). One can here recall that such investigation directly relies on theoretical developments and outcomes that had been achieved by the present authors in [14], where the signal degradation induced by centered Lagrange interpolation schemes had been characterized thanks to a dedicated analysis of their spuriousing and subsequent aliasing mechanisms.

5.1 Theoretical analysis of centered spectral-like optimized interpolation schemes

In order to assess the signal degradation features of centered spectral-like optimized interpolation schemes introduced at Subsection 4.1, let us express their respective and so-called $c_{\Delta x_1}(\cdot)$ function (which characterizes all interpolation features, see Appendix A), and compare it against the one associated with their standard counterpart. For doing so, the various sets of scheme's coefficients $S_j(\cdot)$ are inserted into the $c_{\Delta x_1}(\cdot)$ expression (see Eq. (A.3)), which spectrum norm is then determined via a normalized Fourier transform $|\mathcal{F}[c_{\Delta x_1}](\cdot)|/\Delta x_1$.

Fig. 6 plots the spectrum norm $|\mathcal{F}[c_{\Delta x_1}](\alpha)|/\Delta x_1$ of the respective $c_{\Delta x_1}(\cdot)$ functions characterizing both the standard and the spectral-like optimized versions of the centered 7-point interpolation scheme (see Section 4.1). As one can see, their standard version exhibits a $c_{\Delta x_1}(\cdot)$ function which spectrum norm (plotted in line) matches the *ideal* interpolation one (in dashed-dotted line) over only one half of the resolved wavenumber range (given by $\alpha \in]-\pi/\Delta x_1, \pi/\Delta x_1[$). Outside this particular zone, the $c_{\Delta x_1}(\cdot)$ function deviates from the *ideal* interpolation one. As explained in [14], this fact directly translates the degradation to be induced by the present interpolation scheme onto signals it

https://doi.org/10.4208/cicp.060515.161115b Published online by Cambridge University Press

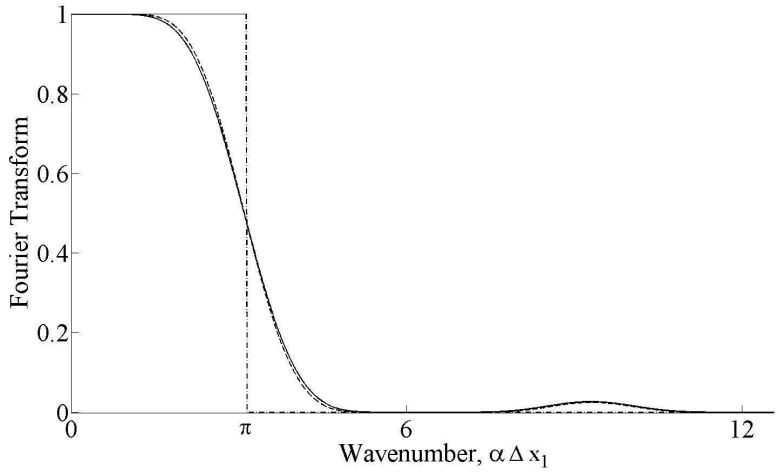


Figure 6: $|\mathcal{F}[c_{\Delta x_1}](\cdot)|/\Delta x_1$. Spectrum norm of $c_{\Delta x_1}(\cdot)$ function associated with a centered 7-point interpolation scheme of either standard (solid line) or spectral-like optimized (dashed line) natures. In dashed-dotted line, the $\mathcal{F}[h_{\Delta x_1}](\cdot)/\Delta x_1$ function, which would correspond to an *ideal* interpolation operator. Please, note that, given the even nature of $|\mathcal{F}[c_{\Delta x_1}](\cdot)|/\Delta x_1$, only half of the spectrum is depicted here.

is applied on. More precisely, the progressive loss in amplitude that $|\mathcal{F}[c_{\Delta x_1}](\alpha)|/\Delta x_1$ exhibits over the $\alpha \in]-\pi/\Delta x_1, \pi/\Delta x_1[$ wavenumber range is directly associated with the alteration of correct information such interpolation scheme will induce onto that part of the signal which is resolved by the donor grid. On another hand, the non identically null values that such $|\mathcal{F}[c_{\Delta x_1}](\alpha)|/\Delta x_1$ function takes over the $\alpha \notin]-\pi/\Delta x_1, \pi/\Delta x_1[$ interval is associated with the creation of incorrect information (i.e. spurious modes generation) such interpolation will induce onto that part of the interpolated signal (step #1) that is not resolved by the donor grid (but that may be aliased when the signal will be projected onto the receiver grid – step #2).

By examining further the same Fig. 6, one can see that, over the range $\alpha \in]-\pi/\Delta x_1, \pi/\Delta x_1[$, its spectral-like optimization improves the interpolation scheme in a very negligible way, with a $|\mathcal{F}[c_{\Delta x_1}](\cdot)|/\Delta x_1$ that gets just very slightly closer to the *ideal* interpolation one ($|\mathcal{F}[h_{\Delta x_1}](\cdot)|/\Delta x_1$, whose norm is plotted in dashed-dotted line). This explains the observations made at Section 4.1 about the quasi negligible gain brought to centered interpolation schemes by their spectral-like optimization, which had confirmed the conclusions intially drawn in [10]. On another hand, when considering the $\alpha \notin]-\pi/\Delta x_1, \pi/\Delta x_1[$ range, one can see that its spectral-like optimization does not really modify (i.e. improve nor degrade) the interpolation scheme, which $|\mathcal{F}[c_{\Delta x_1}](\cdot)|/\Delta x_1$ function also remains roughly the same. In particular, one can see that the optimization procedure leaves almost unchanged the $|\mathcal{F}[c_{\Delta x_1}](\cdot)|/\Delta x_1$ function's wave pockets (which, as demonstrated in [14] and recalled in Appendix A, are responsible for the spurious modes generation).

In addition, by observing now the real and imaginary parts of such $\mathcal{F}[c_{\Delta x_1}](\cdot)$ func-

https://doi.org/10.4208/cicp.060515.161115b Published online by Cambridge University Press

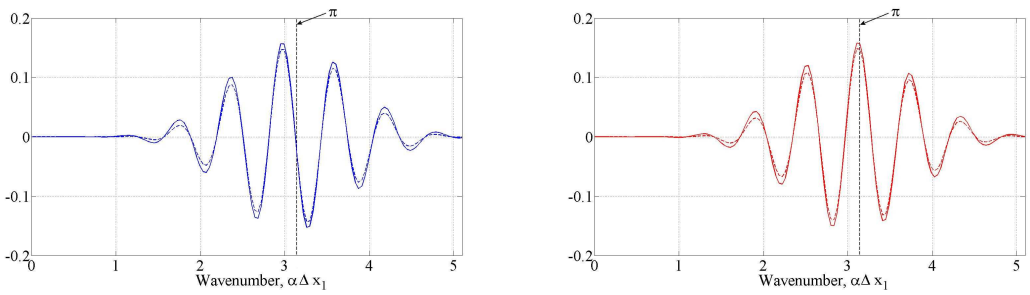


Figure 7: (a) Real and (b) imaginary parts of the phase-shift error E_ϕ induced by centered 7-point interpolation schemes of either standard (solid lines) or spectral-like optimized (dashed lines) natures.

tion, one can see that its spectral-like optimization does not improve that much the phase-shift features of the interpolation scheme. As an illustration, Figs. 7(a) and 7(b) respectively plot the real and the imaginary parts of the phase-shift error E_ϕ to be induced by both schemes, with such quantity defined as:

$$E_\phi(\alpha) = \frac{\mathcal{F}[c_{\Delta x_1}](\alpha)}{\Delta x_1} - \frac{|\mathcal{F}[c_{\Delta x_1}](\alpha)|}{\Delta x_1} e^{i\alpha}. \tag{5.1}$$

By examining how such error behaves over the higher part of the spectrum, one can conclude that the present 7-point interpolation scheme is likely to induce a phase-shift of high-wavenumber contents, wheter it has been spectral-liked optimized or not. At this stage, one can recall that phase-shift phenomena to be induced by an interpolation can be avoided only if the latter is composed of a centered scheme with an *even* number of stencil points [14] (which was not the case in [10] and, thus, here).

5.2 Theoretical analysis of noncentered spectral-like optimized interpolation schemes

Analogously to what was done for its centered counterpart, Fig. 8 compares the $|\mathcal{F}[c_{\Delta x_1}](\cdot)|/\Delta x_1$ functions associated with both the standard and the spectral-like optimized versions of the noncentered 7-point interpolation (cf. Subsection 4.2).

By examining this figure, one can make several observations and draw various conclusions. First of all, and similarly to what happened for its centered counterpart, the present noncentered standard 7-point interpolation exhibits a $c_{\Delta x_1}(\cdot)$ function whose spectrum norm $|\mathcal{F}[c_{\Delta x_1}](\alpha)|/\Delta x_1$ (plotted in line) matches the *ideal* interpolation one (plotted in dashed-dotted line) over approximately half of the resolved frequency range, after what it deviates from it. On that point however, and contrarily to what happened in the previous (centered standard scheme) case, such spectrum norm function takes values that largely exceed the unity over a non negligible part of the $\alpha \in]-\pi/\Delta x_1, \pi/\Delta x_1[$ (i.e. resolved) range. This explains why noncentered interpolation schemes such as this one

https://doi.org/10.4208/cicp.060515.161115b Published online by Cambridge University Press

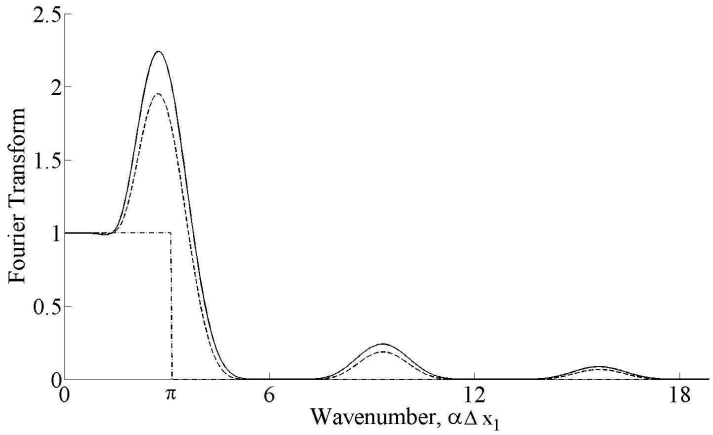


Figure 8: $|\mathcal{F}[c_{\Delta x_1}](\cdot)|/\Delta x_1$. Spectrum norm of $c_{\Delta x_1}(\cdot)$ function associated with noncentered 7-point interpolation of either standard (solid line) or spectral-like optimized (dashed line) nature. In dashed-dotted line, the $\mathcal{F}[h_{\Delta x_1}](\cdot)/\Delta x_1$ function, which would correspond to an *ideal* interpolation operator. Please, note that, given the even nature of $|\mathcal{F}[c_{\Delta x_1}](\cdot)|/\Delta x_1$, only half of the spectrum was depicted here.

are likely to amplify some of the well-resolved contents of the signal they are applied to. Additionally, over the non resolved wavenumber range (i.e. $\alpha \notin]-\pi/\Delta x_1, \pi/\Delta x_1[$), this spectrum norm function also exhibits *spuriousing* wave pockets, which magnitude is more important than in the previous (centered standard interpolation) case. All this indicates that, when applied to a signal, noncentered standard interpolation schemes are not only likely to amplify its high frequency contents, but also to spurious it more importantly than their centered counterpart.

Now, by comparing the previous noncentered standard interpolation $|\mathcal{F}[c_{\Delta x_1}](\alpha)|/\Delta x_1$ curve with that of its spectral-like optimized counterpart (plotted in dashes, on the same Fig. 8), one can understand why, although it has some beneficial effects on it, its spectral-like optimization cannot prevent a given noncentered interpolation to possibly (i) amplify and (ii) spurious part of the signal it is applied to. Indeed, as one can see, the scheme' spectrum norm $|\mathcal{F}[c_{\Delta x_1}](\alpha)|/\Delta x_1$ is only slightly impacted by the spectral-like optimization process, which leaves it roughly unchanged.

Regarding now the phase-shift phenomenon to be possibly induced by these two noncentered interpolation schemes, Figs. 9(a) and 9(b) respectively depict the real and imaginary parts of the associated error E_ϕ. Here again, although it is more important than in the case of a centered interpolation, the gain brought by the spectral-like optimization is still insufficient for improving the present noncentered 7-point interpolation scheme in a significant way.

Now, let us replace the spectral-like optimized noncentered interpolation previously assessed with its improved version, which is based on the amplification control technique recalled above. Similarly to what was presented just before, Fig. 10 compares the $|\mathcal{F}[c_{\Delta x_1}](\cdot)|/\Delta x_1$ functions associated with the noncentered 6-point interpolation

https://doi.org/10.4208/cicp.060515.161115b Published online by Cambridge University Press

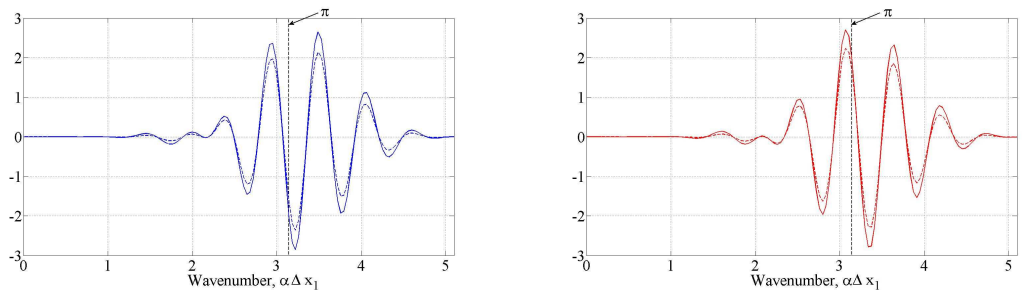


Figure 9: (a) Real and (b) imaginary parts of the phase-shift error E_ϕ induced by noncentered 7-point interpolation schemes of either standard (solid lines) or spectral-like optimized (dashed lines) natures.

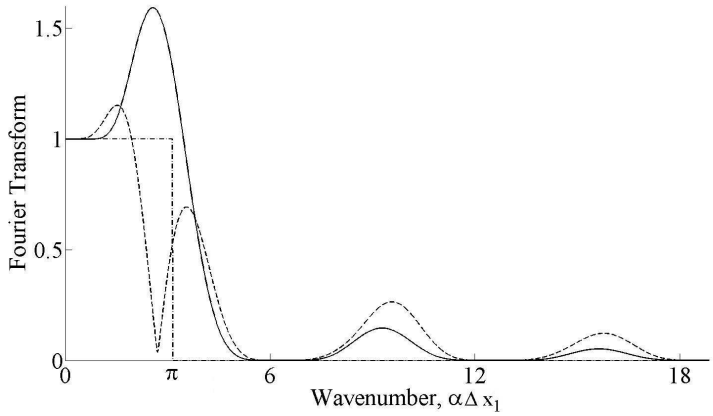


Figure 10: $|\mathcal{F}[c_{\Delta x_1}](\cdot)|/\Delta x_1$. Spectrum norm of $c_{\Delta x_1}(\cdot)$ function associated with a noncentered 6-point interpolation of either standard (solid line) or spectral-like optimized with amplification control (dashed line) nature. In dashed-dotted line, the $\mathcal{F}[h_{\Delta x_1}](\cdot)/\Delta x_1$ function, which would correspond to an *ideal* interpolation. Please, note that, given the even nature of $|\mathcal{F}[c_{\Delta x_1}](\cdot)|/\Delta x_1$, only half of the spectrum is depicted here.

(cf. Subsection 4.2.2) of either standard (plotted in lines) or spectral-like optimized with amplification control (in dashes) nature. By examining this figure, one can first notice that, compared to its standard counterpart, the present spectral-like optimized with amplification control interpolation exhibits a $c_{\Delta x_1}(\cdot)$ function whose spectrum norm $|\mathcal{F}[c_{\Delta x_1}](\alpha)|/\Delta x_1$ rarely exceeds the critical unitary value. This explains why this particular spectral-like optimization technique effectively helps in minimizing the amplification side-effect associated with noncentered interpolations.

On another hand, compared to that of its standard counterpart, such spectrum norm deviates sooner from the ideal interpolation one. This indicates that, contrarily to the baseline spectral-like optimization technique, the present amplification control-based approach may lead noncentered interpolations to more importantly degrade (in terms of alteration of the correct information) all signal components that are well-resolved. Ad-

https://doi.org/10.4208/cicp.060515.161115b Published online by Cambridge University Press

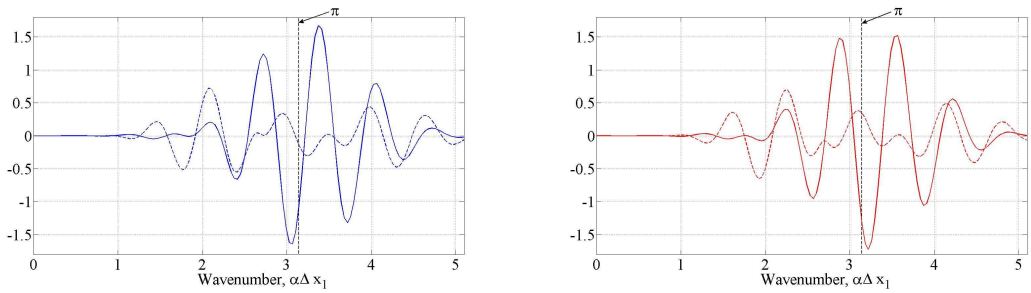


Figure 11: (a) Real and (b) imaginary parts of the phase shift error E_ϕ induced by noncentered 6-point interpolation schemes of either standard (solid lines) or spectral-like optimized with amplification control (dashed lines) nature.

ditionally, concerning now that part of the signal which is not resolved, the degradation (in terms of spurious modes generation, this time) is also to be enhanced by this particular spectral-like optimization technique. This, indeed, can be inferred from what happens over the unresolved wavenumber range ($\alpha \notin]-\pi/\Delta x_1, \pi/\Delta x_1[$), over which the $|\mathcal{F}[c_{\Delta x_1}](\cdot)|/\Delta x_1$ function exhibits wavepockets of higher magnitude, compared to those associated with the baseline spectral-like optimization. Finally, this amplification control-based spectral-like optimization technique also enhances the phase shift error by noncentered interpolation schemes, as can be inferred from Figs. 11(a) and 11(b).

6 Further insights on the spurious modes generation by interpolation schemes

As was assessed and analyzed in the previous sections, their spectral optimization may slightly enhance the accuracy of interpolation schemes over part of their well-resolved frequency range. However, as was also shown, none of the various spectral-like optimization techniques really improve the interpolators' behavior in terms of spurious modes minimization.

With the view of (i) better understanding and (ii) potentially removing such inability of spectral-like optimization procedures to minimize the spurious modes generation by interpolation schemes, in the present section, the theoretical investigations conducted above are further developed. The first objective is to derive a particular optimization constraint, to be explicitly related to the minimization of these interpolation errors that are specifically induced by the signal degradation mechanisms. The goal is then to highlight how, because they fail in integrating such specific constraint among their optimization criteria, spectral-like optimized interpolation schemes presented above can not escape degrading signals they are applied to in terms of spurious modes generation.

https://doi.org/10.4208/cicp.060515.161115b Published online by Cambridge University Press

6.1 Harmonic analysis – generic form

First of all, for preventing an interpolation scheme to degrade a given signal by polluting it with incorrect information, it is first needed to accurately determine *when* and *how* its associated spurious mode generation phenomenon may arise. For doing so, let us apply a given interpolation operator to a single harmonic component of the form $f(x)=e^{ikx}$, with $k\in]-\pi/\Delta x_1,\pi/\Delta x_1[$. In this particular (harmonic) case, the generic *interpolated signal* expression given by Eq. (2.1) reduces to:

$$\mathcal{I}[e^{ikx}](x)=\sum_{n=-\infty}^{+\infty}\mathbf{1}_{[0,1[}\left(\frac{x}{\Delta x_1}-n\right)\sum_{j=J_{\min}}^{J_{\max}}S_j\left(\frac{x}{\Delta x_1}-n\right)e^{(n+j)k\Delta x_1}. \tag{6.1}$$

By taking the Fourier transform of the previous quantity, and after a few manipulations involving, among others, identities of Appendix A, one gets the interpolated signal spectrum:

$$\begin{aligned}\mathcal{F}[\mathcal{I}[e^{ikx}]](\alpha)=&\underbrace{\frac{2\pi\mathcal{F}[c_{\Delta x_1}](\alpha)}{\Delta x_1}\delta(\alpha-k)}_{\text{term }\neq 0\text{ only for }\alpha=k}\\&+\underbrace{\frac{2\pi\mathcal{F}[c_{\Delta x_1}](\alpha)}{\Delta x_1}\sum_{\substack{n=-\infty\\n\neq 0}}^{+\infty}\delta\left(\alpha-k-\frac{2\pi n}{\Delta x_1}\right)}_{\text{term }\neq 0\text{ for various }\alpha\notin]-\pi/\Delta x_1,\pi\Delta x_1[},\quad\forall\alpha\in]-\infty,\infty[.\end{aligned} \tag{6.2}$$

In the above expression, the first term (which is nonzero for $\alpha=k$ only) corresponds to the original signal fundamental frequency.

In the present *harmonic* case, if the interpolation was of *ideal* nature, such interpolated signal spectrum would gather nothing else than this sole component, which expression would then correspond to that of the ideal interpolation, that is, the one associated with $h_{\Delta x_1}(\cdot)$ function, with Eq. (6.2) becoming then:

$$\mathcal{F}[\mathcal{I}[e^{ikx}]](\alpha)=\frac{2\pi\mathcal{F}[h_{\Delta x_1}](\alpha)}{\Delta x_1}\delta(\alpha-k),\quad\forall\alpha\in]-\infty,\infty[. \tag{6.3}$$

Now, one could ever imagine that, although it is not of ideal nature, a given interpolation could be free of any spurious mode generation, its signal degradation features being then restricted to the sole alteration of correct information. In that case, the previous Eq. would become

$$\mathcal{F}[\mathcal{I}[e^{ikx}]](\alpha)=\frac{2\pi\mathcal{F}[c_{\Delta x_1}](\alpha)}{\Delta x_1}\delta(\alpha-k),\quad\forall\alpha\in]-\infty,\infty[. \tag{6.4}$$

In other words, a sufficient condition for the interpolation to ideally behave in terms of spurious modes generation would be that the second term at the right-hand-side of

https://doi.org/10.4208/cicp.060515.161115b Published online by Cambridge University Press

Eq. (6.2) is identically zero. Such term indeed corresponds to all spurious modes that may be generated over the unresolved part of the frequency range and possibly further aliased back onto its resolved part, when projected onto a receiver grid – all this because of the non-ideal nature of the interpolation.‡

Therefore, for an optimization technique effectively minimizes the spurious modes generation mechanisms by a given interpolation, it would at least be needed that the optimization process acts in some way onto such second term of the interpolated signal spectrum. This indeed does not seem to be the case with spectral-like optimization approaches, which do not reduce (and, sometimes, even magnify) the amount of spurious modes generated by interpolation schemes, as was numerically assessed in Section 4, and theoretically demonstrated in Section 5.

With the view of investigating that point further, in the following, the harmonic analysis that was here conducted is compared against the (somehow more restrictive) one on which spectral-like optimizations were originally based.

6.2 Harmonic analysis – alternative form

First, let us express Eq. (6.1) in an alternative manner, by considering that $x \in [n\Delta x_1,(n+1)\Delta x_1[$ for a given $n \in \mathbb{N}$. Introducing now the variable change $\eta(x)=x/\Delta x_1-n$, one gets:

$$\mathcal{I}[e^{ikx}](x) = \underbrace{\left[\sum_{j=J_{\min}}^{J_{\max}} S_j(\eta) e^{ik\Delta x_1(j-\eta)}\right]}_{T_F(k\Delta x_1,\eta)} e^{ikx}, \quad \eta \in [0,1[. \tag{6.5}$$

In the previous expression, the term into brackets corresponds to the interpolation's *local* transfer function, here defined as $T_F(\cdot,\cdot)$. An ideal interpolation scheme would obviously be characterized by a unitary local transfer function, that is $T_F(k\Delta x_1,\eta) = 1$, $\forall k \in]-\pi/\Delta x_1,\pi,\Delta x_1[$ and $\forall \eta \in [0,1[$. This, however, is never achieved in practice, and $T_F(k\Delta x_1,\eta) \neq 1$ for some harmonic components of high wavenumber k in $]-\pi/\Delta x_1,\pi/\Delta x_1[$. The principle of spectral-like optimization techniques is indeed to determine the optimal set(s) of $S_j(\cdot)$ such that the T_F-associated integrated error can be minimized over a given frequency range $[-k,k] \subset]-\pi/\Delta x_1,\pi/\Delta x_1[$ (see, for instance, Eqs. (4.1) and (4.5)).

Now, submitting Eq. (6.5) to a Fourier transform, one can relate the interpolation' spectrum with that of its local transfer function:

$$\mathcal{F}[\mathcal{I}[e^{ikx}]](\alpha) = \mathcal{F}[T_F](k\Delta x_1,\alpha-k), \quad \forall \alpha \in]-\infty,\infty[. \tag{6.6}$$

‡All of the theoretical results established here were derived with respect to interpolation, i.e under the assumption that Eq. (2.1) represents an interpolation operator. They can however be readily extended to extrapolation operators provided that assumptions made on intervals of j and n do not question the applicability of the Signal Theory's theorems used here. One can thus infer that extrapolation processes are as likely as interpolation ones to suffer from the spuriousing (and its subsequent aliasing) side-effect.

https://doi.org/10.4208/cicp.060515.161115b Published online by Cambridge University Press

Finally, by making use of Eq. (6.2), one can express the latter interpolation's local transfer function spectra in terms of the $c_{\Delta x_1}(\cdot)$ function:

$$\mathcal{F}[T_F](k\Delta x_1,\alpha-k)=\underbrace{\frac{2\pi\mathcal{F}[c_{\Delta x_1}](\alpha)}{\Delta x_1}\delta(\alpha-k)}_{\text{term}\neq 0\text{ only for }\alpha=k}+\underbrace{\frac{2\pi\mathcal{F}[c_{\Delta x_1}](\alpha)}{\Delta x_1}\sum_{\substack{n=-\infty\\ n\neq 0}}^{+\infty}\delta\left(\alpha-k-\frac{2\pi n}{\Delta x_1}\right)}_{\text{term}\neq 0\text{ for various }\alpha\notin]-\pi/\Delta x_1,\pi\Delta x_1[},\quad \forall\alpha\in]-\infty,\infty[. \tag{6.7}$$

Considering now what was discussed in Section 6.1, one can conclude that a *spurious modes-free* interpolation scheme would require that the second term at the right-hand-side of Eq. (6.7) is zero, that is to say, its local transfer function spectrum should be solely composed of the original signal's fundamental frequency:

$$\mathcal{F}[T_F](k\Delta x_1,\alpha-k)=\frac{2\pi\mathcal{F}[c_{\Delta x_1}](\alpha)}{\Delta x_1}\delta(\alpha-k),\quad \forall\alpha\in]-\infty,\infty[. \tag{6.8}$$

Needless to say, any optimization procedure that seeks at improving interpolations should integrate this kind of condition, such that resulting interpolation schemes effectively behave better than standard ones, in terms of spurious modes generation[§]. This was not the case for spectral-like optimization techniques detailed above.

On that stage, however, it is important to underline that the previous identity can be verified by *any* interpolation scheme, from the moment it is used *under specific conditions*. As an example, whenever the interpolation's transfer function associated with the donor and receiver grids is a function of $k\Delta x_1$ only, i.e. $T_F(k\Delta x_1,\eta)=g(k\Delta x_1)$, one can write

$$\mathcal{F}[T_F](k\Delta x_1,\alpha-k)=g(k\Delta x_1)\delta(\alpha-k),\quad \forall\alpha\in]-\infty,\infty[. \tag{6.9}$$

In such a situation, no creation of incorrect information (i.e. spurious mode generation) can be induced by the interpolation scheme, which signal degradation is therefore restricted to the sole alteration (i.e. dissipation, amplification or dispersion) of the signal original components. In other words, *whatever its interpolation basis $S_j(\cdot)$ is, a given interpolation may see its spurious mode generation features blocked* from the moment its associated local transfer function, $T_F(k\Delta x_1,\eta)$, is function of the dimensionless wavenumber, $k\Delta x$, only. Therefore, whenever a given interpolation is assessed under such kind of special circumstances, its associated spuriousing phenomena remains *ineffective*. In particular, this is what happened with the validation cases of spectral-like optimization techniques provided in [10, 12], as is shown in the next section.

[§]One can here precise that, based on all these outcomes, a specific study was conducted, which resulted in developing an innovative optimization technique leading to interpolations of minimal spurious modes generation [17].

https://doi.org/10.4208/cicp.060515.161115b Published online by Cambridge University Press

7 On the relative validity of validation exercises proposed for spectra-like optimized interpolation schemes

Indeed, at this stage, it is legitimate to wonder how spectral-like optimized schemes might misbehave, if one consider the validation exercises through which such schemes had been originally assessed in [10,12].

With the view of answering such question, thereafter, the particular configurations used by their respective authors for validating the spectral-like optimized schemes they proposed [10,12] are investigated. The objective here is to assess how far these validation cases were likely to reveal the spurious noise generation (and subsequent aliasing) that spectral-like optimized schemes appear to be subjected to.

7.1 Optimized extrapolation and interpolation schemes for immersed boundary conditions

In [10], an Immersed Boundary Condition (IBC) was proposed, for which spectral-like optimized interpolation and extrapolation schemes were developed. Fig. 12 sketches in $1D$ the IBC principle, thanks to which a signal known onto a set of donor grid points can be extrapolated towards a non-coincident wall point indicated by the relative coordinate η. Based on such wall extrapolated value, the boundary condition is then enforced via the last and so-called ghost point of the grid. One can here notice that, in this particular $1D$ case, the receiver grid is degenerated, gathering the sole wall point of relative coordinate η.

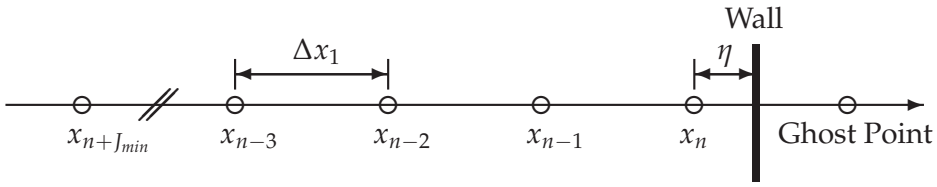


Figure 12: $1D$ configuration illustrating the Immersed Boundary Condition of [10].

Let us now consider that a given harmonic signal of dimensionless wavenumber $k\Delta x_1$ propagates on such $1D$ grid, and is thus to be extrapolated onto the wall points as it approaches the boundary. In such a purely *harmonic* case, the extrapolated signal spectrum is simply given by the extrapolation scheme transfer function $T_F(k\Delta x_1,\eta)$, for a well-defined η. It is obvious that such transfer function depends on $k\Delta x_1$ *only* and, thus, that Eq. (6.9) is automatically verified, meaning that *no spurious modes generation may occur*. Therefore, in this particular case, the signal degradation only consists in the possible alteration of well-resolved components (i.e. those such that $k\in]-\pi/\Delta x_1,\pi,\Delta x_1[$), a configuration for which the spectral-like optimization is effectively of help.

https://doi.org/10.4208/cicp.060515.161115b Published online by Cambridge University Press

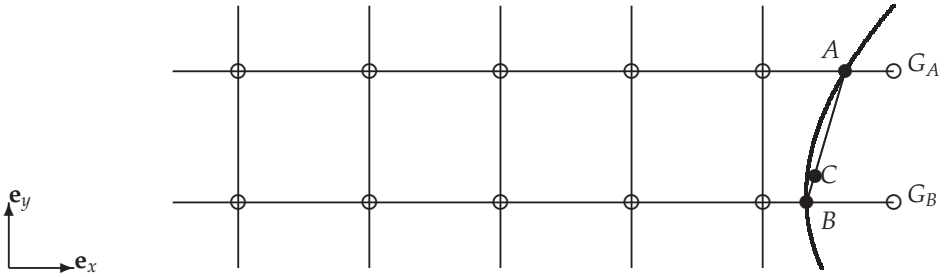


Figure 13: $2D$ curvilinear extension of the $1D$ configuration depicted in Fig. 12. Points B (resp. A) corresponds to the intersection between the wall and the donor grid line, while G_B (resp. G_A) is the ghost point where the boundary condition is to be enforced, via point C (such that $\overline{CG_B} \perp \overline{AB}$).

Now, let us consider the $2D$-curvilinear equivalent of the previous case with a curved solid wall sunk within a bi-dimensional Cartesian homogeneous grid of discretization steps Δx and Δy, as depicted in Fig. 13. In this case, the IBC treatment [18] still begins with a $1D$ extrapolation (i.e. along x-lines) of the propagated signal towards the wall points A and B. From the latter points, the segment $\overline{AB}$ approximating the curve $\overset{\frown}{AB}$ is drawn, from which the point C such that $\overline{CG_B} \perp \overline{AB}$ is then determined. Finally, once the extrapolated signal of A- and B-wall points has been interpolated onto it, such point C allows enforcing the boundary condition at ghost point G_B. Needless to say, since the previous approach relies on a linear approximation of curve segments ($\overline{AB}$ vs $\overset{\frown}{AB}$), the denser the mesh is, and the better the IBC will behave. Although necessary, such condition may not be sufficient for ensuring that this particular IBC technique is accurate enough, as will be shown below.

Indeed, let us consider again a harmonic signal of dimensionless wavenumber $k\Delta x$ that propagates in the x-direction, and that is to be extrapolated as it reaches A and B wall points. As previously, in such a *harmonic* case, the extrapolated signal spectrum at point A (resp. B) is given by the extrapolation scheme's transfer function $T_F(k\Delta x,\eta_A)$ (resp. $T_F(k\Delta x,\eta_B)$). Contrarily to what happened before, however, such function is *no longer dependent of $k\Delta x$ only*, that is, it will not deliver the same value, depending on the wall point considered. Therefore, Eq. (6.9) may not be verified, meaning that *spurious modes generation may occur*, depending on the signal dimensionless wavenumber $k\Delta x$. As an example, the spectral-like optimized extrapolation scheme proposed in [18] was designed to accurately predict wavenumbers up to 8 points-per-wavelength (PPW) [18]. One can thus consider that for signal components of more than 8 PPW, $T_F(k\Delta x,\eta_A) \cong T_F(k\Delta x,\eta_B)$, that is, the spurious modes to be generated will be negligible.

On another hand, for signal components such that $k\Delta x$ is less than 8 PPW, the assumption $T_F(k\Delta x,\eta_A) \cong T_F(k\Delta x,\eta_B)$ no longer holds, that is, spurious modes to be generated have no reason to be negligible. In particular, since the extrapolation scheme is here of noncentered nature, one can expect both high-wavenumber contents and spurious modes to be amplified, a thing that the signal dissipation to be possibly induced by the $A+B \to C$

https://doi.org/10.4208/cicp.060515.161115b Published online by Cambridge University Press

linear interpolation step may be far insufficient to remedy.

From a more global point-of-view, it is important to notice that the latter situation may occur *whatever the frequency of the signal is*, from the moment the later propagates in another direction than the x-axis. Indeed, in those cases where the propagating direction deviates from the grid lines one, the signal wavenumber k decomposes itself into k_x and k_y components (with $k=\sqrt{k_x^2+k_y^2}$), with the latter components taking any value between 0 and k. On another hand, for the extrapolation stage does not generate spurious modes, the criteria enunciated above for $k\Delta x_1$ is now to be verified by $k_x\Delta x$ *and* $k_y\Delta y$. Therefore, unless both conditions are verified at the same time, the IBC extrapolation stage is likely to generate spurious modes.

7.2 Optimized interpolation schemes and overlapping grids

In [12], various spectral-like optimized interpolations were assessed, thanks to a dedicated test case that relied on two $1D$ *identical* and *homogeneous* grids overlapping each other. On the first grid, a signal consisting of a low-wavenumber wave-packet was convected through the $1D$ convection equation, while being artificially polluted with a spurious mode given by a low-amplitude high-wavenumber wave-packet, to be forced through the convection equation source term. Such polluted signal was then transferred from the first to the second grid via noncentered spectral-like optimized interpolation schemes, either with or without amplification control. The data transfer to occur from the second to the first grid was carried out via a centered Lagrange interpolation.

The authors showed that, when the interpolation stage was conducted with noncentered spectral-like optimized schemes without amplification control, the signal saw its high-frequency mode being amplified until the simulation blew up. On another hand, when noncentered amplification control-based optimized interpolations were used instead, the simulation remained stable, and delivered the expected results.

On that stage, however, one can again underline that such a validation exercise does not seem to have been of sufficient generality for allowing to properly assess *all* side-effects by interpolations, such as the spurious mode generation. More precisely, the simple fact that such interpolation operation was conducted between two translated *identical* and *homogeneous* grids prevented it from generating any spurious mode. Indeed, here again, the interpolated signal was defined by the interpolation scheme's transfer function, which – in such particular configuration – was dependent of the dimensionless wavenumber only. As for the previous case (see Section 7.1), this implied that Eq. (6.9) was automatically verified, that is, *no spurious modes generation could occur*.

In order to illustrate that point from a more global perspective, let us extend in two dimensions the particular $1D$ configuration proposed in [12]. For doing so, let us consider two identical homogeneous Cartesian $2D$ grids, to be simply translated along both x- and y-directions by a vector (η_x,η_y) (see Fig. 14).

Now, let us consider that one transfers a harmonic signal from one grid to the other, by making use of interpolations. Whatever the x- (resp. y-) interpolation scheme to be

https://doi.org/10.4208/cicp.060515.161115b Published online by Cambridge University Press

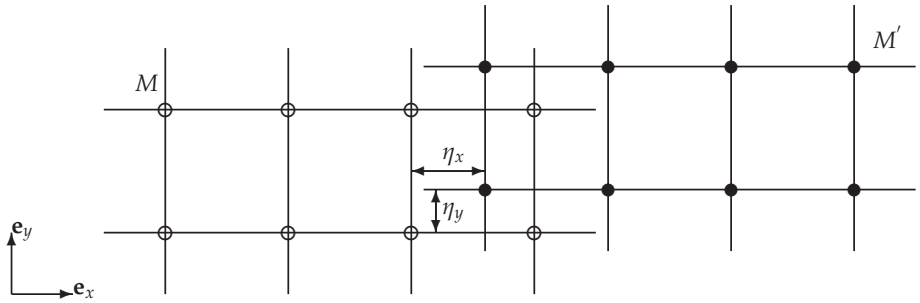


Figure 14: $2D$ extension of the $1D$ configuration proposed in [12], with two *identical* and *homogeneous* Cartesian grids overlapping each other, while departing from a vector (η_x,η_y).

used is, for all receiver points and for all $k_x \in]-\pi/\Delta x,\pi/\Delta x[$ (resp. $k_y \in]-\pi/\Delta y,\pi/\Delta y[$), the interpolation's transfer function solely depends on the dimensionless wavenumber $k\Delta x$ (resp. $k\Delta y$), always taking the same identical $T_F(k\Delta x,\eta_x)$ (resp. $T_F(k\Delta y,\eta_y)$) value. As a result, for both directions, no spurious modes can be generated by the interpolation process, which signal degradation effect is then solely composed of all dissipation (for centered schemes) or amplification (for noncentered schemes) phenomena to occur over the higher part of the frequency range (besides the dispersion phenomenon).

On another hand, it is clear that the improvements brought by the spectral-like optimized interpolation schemes may no longer hold from the moment the above *homogeneous* Cartesian grids are replaced with *heterogeneous* (e.g. stretched) ones, which is likely to occur when realistic problems are to be addressed. Indeed, in that case, the interpolation's transfer functions may no longer depend on the dimensionless wavenumber only, since it *also* varies with the local (η_x,η_y) donor-to-receiver grids shift[¶]. Therefore, the interpolation process is likely to induce some spurious mode generation (and subsequent aliasing) over that part of the frequency range which would not meet the specific criteria that were proposed by the present authors in a previous work (see [14]).

8 Conclusion

The present work focused on the effective accuracy of interpolation schemes to be used within a Computational Acoustics context. With that view, the so-called *spectral-like* optimized interpolation schemes were analyzed, with respect to the signal degradation any aeroacoustic signal maybe subjected to, when submitted to a given interpolation process.

[¶]On that stage, it is important to notice that, concerning each receiver point's relative location with respect to its immediate surrounding donor points, there is a perfect bijection between the physical domain (where the donor mesh is possibly heterogeneous and curvilinear) and the computational one (where it is, on the contrary, of homogeneous and Cartesian nature). This being verified, any consideration that can be made in the physical domain about the relative location (and, thus, the local transfer function $T_F(\cdot,\cdot)$) finds a direct and immediate translation in the computational one, where the present theoretical analysis and outcomes apply.

https://doi.org/10.4208/cicp.060515.161115b Published online by Cambridge University Press

First, it was here shown that such signal degradation by a given interpolation operator consists not only in the (i) alteration (via either dissipation, amplification or dispersion effects) of the signal's original content, but also in its (ii) corruption by the so-called *spuriousing* and subsequent *aliasing* phenomena. It was then recalled how interpolation schemes, whether they are of centered or noncentered kind, are likely to degrade aeroacoustic signals they are applied to [14]. More important, it was demonstrated that, although their spectral-like optimization may effectively improve interpolation schemes in some way, it cannot really help in minimizing their signal degradation features, whether the latter are induced by an alteration or by a corruption of the interpolated contents. On that stage, it was shown how the various spectral-like optimized interpolation schemes that were considered here had been initially validated by their authors on the basis of specific test cases, which particular set up prevented the spurious modes generation to occur.

All these outcomes were drawn thanks to assessment exercises relying on academic test cases, as well as to theoretical developments based on an original formalism by the present authors [14]. Among other things, the latter formalism allowed here to determine (i) what criteria shall better be respected by a given interpolation scheme for not generating spurious modes, and (ii) how any of the proposed spectral-like optimization failed in integrating such criteria within its optimization constraints.

On that stage, one can notice that, thanks to the generality of the theoretical formalism it relies on, the present study could easily be extended to other types of interpolation schemes (e.g. spline interpolations). In addition, part of these theoretical outcomes, such as the $c_{\Delta x}(\cdot)$ function formalism, could be of great help for developing innovative optimization procedures that would deliver interpolation processes (and, thus, schemes) with minimal signal degradation features. As an example, within another framework, the present authors developed a novel (and non spectral-based) optimization procedure, which was then validated via a direct application to academic and realistic test cases [17].

A The interpolation under the point of view of the signal theory

Let us consider a square-integrable function $f:\mathbb{R}\longmapsto\mathbb{R}$. According to the convention used in the present study, its Fourier transform is given by:

$$\mathcal{F}[f](\alpha)=\int_{-\infty}^{+\infty}f(x)e^{-i\alpha x}dx, \tag{A.1}$$

where α is a given wavenumber. The fundamental result of the Signal Theory states that, if the support of $\mathcal{F}[f](\cdot)$ is included in $\left]\frac{-\pi}{\Delta x_1},\frac{\pi}{\Delta x_1}\right[$, then the function f can be written as a convolution product [13]:

$$f(x)=\sum_{n=-\infty}^{+\infty}f(n\Delta x_1)h_{\Delta x_1}(x-n\Delta x_1)=f_d*h_{\Delta x_1}(x), \tag{A.2}$$

https://doi.org/10.4208/cicp.060515.161115b Published online by Cambridge University Press

where $f_d(x)=\sum_{-\infty}^{\infty} f(n\Delta x_1)\delta(x-n\Delta x_1)$ is the discretized form of $f(\cdot)$ and $h_{\Delta x_1}(x)=\frac{sin(\pi x/\Delta x_1)}{\pi x/\Delta x_1}$. Considering now that interpolating a function can be seen as reconstructing it with the help of specific interpolation basis, it appears that $h_{\Delta x_1}(\cdot)$ would indeed constitute an *ideal* interpolation. However, in Eq. (A.2) the sum over n is infinite and cannot thus be truncated arbitrarily. Therefore, it is more indicated to replace $h_{\Delta x_1}(\cdot)$ by a finite set of interpolators, $c_{\Delta x_1}(\cdot)$, to be defined as [8]:

$$c_{\Delta x_1}(x)=\sum_{j=J_{\min}}^{J_{\max}} \mathbf{1}\left(\frac{x}{\Delta x_1}+j\right) S_j\left(\frac{x}{\Delta x_1}+j\right). \tag{A.3}$$

In this case, Eq. (2.1) becomes [13]:

$$\mathcal{I}[f](x)=\sum_{n=-\infty}^{+\infty} f(n\Delta x_1)c_{\Delta x_1}(x-n\Delta x_1)=f_d*c_{\Delta x_1}(x). \tag{A.4}$$

Thanks to the presence of the identity function into Eq. (A.3), $\mathcal{I}[f](x)$ has a compact support for a given x, which means that, in practice, the sum over n can be safely truncated. However, one can remark that the interpolation basis $S_j(\cdot)$ shall better be chosen such that $c_{\Delta x_1}(\cdot)$ is close enough to $h_{\Delta x_1}(\cdot)$.

Given that interpolating a given function corresponds to a convolution between the latter and the $c_{\Delta x_1}$ function, the interpolation process can be simply sketched as the following successive steps:

0. discretization of $f(\cdot)$ on the donor grid,

$$f_d(x)=\sum_{n=-\infty}^{+\infty} f(n\Delta x_1)\delta(x-n\Delta x_1), \tag{A.5}$$

1. interpolation of the discretized function, f_d,

$$\mathcal{I}[f](x)=f_d*c_{\Delta x_1}(x), \tag{A.6}$$

2. projection of the interpolated function onto the receiver grid,

$$\mathcal{I}[f]_d(x)=\sum_{n=-\infty}^{+\infty} \mathcal{I}[f](n\Delta x_2)\delta(x-n\Delta x_2). \tag{A.7}$$

Where the subscript $i\in\{1,2\}$ associated with a given variable indicates on which grid it is considered (donor, $i=1$, or receiver, $i=2$).

Taking the Fourier transform of Eqs. (A.5)-(A.7) leads to, respectively:

$$\mathcal{F}[f_d](\alpha)=\frac{1}{\Delta x_1}\sum_{m_1=-\infty}^{\infty} \mathcal{F}[f]\left(\alpha-\frac{2\pi m_1}{\Delta x_1}\right), \tag{A.8}$$

$$\mathcal{F}[\mathcal{I}[f]](\alpha)=\mathcal{F}[f_d](\alpha)\times\mathcal{F}[c_{\Delta x_1}](\alpha), \tag{A.9}$$

$$\mathcal{F}[\mathcal{I}[f]_d](\alpha)=\frac{1}{\Delta x_2}\sum_{m_2=-\infty}^{+\infty} e^{-i\frac{2\pi m_2}{\Delta x_2}d}\mathcal{F}[\mathcal{I}[f]]\left(\alpha-\frac{2\pi m_2}{\Delta x_2}\right), \tag{A.10}$$

https://doi.org/10.4208/cicp.060515.161115b Published online by Cambridge University Press

or, equivalently,

$$\mathcal{F}[\mathcal{I}[f]_d](\alpha)=\frac{1}{\Delta x_1\Delta x_2}\sum_{m_2,m_1=-\infty}^{\infty}e^{-i\frac{2\pi m_2}{\Delta x_2}d}\mathcal{F}[f]\left(\alpha-\frac{2\pi m_1}{\Delta x_1}-\frac{2\pi m_2}{\Delta x_2}\right)\times\mathcal{F}[c_{\Delta x_1}]\left(\alpha-\frac{2\pi m_2}{\Delta x_2}\right). \tag{A.11}$$

Eq. (A.11) contains all the interpolation features, like the mechanisms responsible for (i) the degradation of high-wavenumber contents and (ii) the spurious modes generation and aliasing. By a proper study of such equation, one can draw several conclusions, which only the two principal are enumerated here (for further details, see [14]).

- Over the resolved frequency range, i.e. $\alpha\in]-\pi/\Delta x_1,\pi/\Delta x_1[$, the signal will see its norm $|\mathcal{F}[f](\alpha)|$ (i) conserved if $\frac{\mathcal{F}[c_{\Delta x_1}](\alpha)}{\Delta x_1}\cong 1$, (ii) reduced if $\frac{\mathcal{F}[c_{\Delta x_1}](\alpha)}{\Delta x_1}<1$, (iii) magnified if $\frac{\mathcal{F}[c_{\Delta x_1}](\alpha)}{\Delta x_1}>1$.
- Whenever $\frac{\mathcal{F}[c_{\Delta x_1}](\alpha)}{\Delta x_1}\neq 0$ over the unresolved frequency range, i.e. $\alpha\neq]-\pi/\Delta x_1,\pi/\Delta x_1[$, the signal will see its content polluted by spurious modes.

B Phase shifting induced by interpolation process' step #2

In the present work, all discretization grids are written as $x_i=n_i\Delta x_i$, where $n_i\in\mathbb{Z}$ and $i\in\{1,2\}$. However, if one considers a receiver grid that takes the form $x_2=n_2\Delta x_2+d$, where $n_2\in\mathbb{N}$, $d\neq 0$ and $d\in[-\Delta x_1/2,\Delta x_1/2[$, then a (non unitary) *grid-to-grid dephasing* term, D_ϕ, appears in Eq. (A.11).

$$D_\phi=e^{-i\frac{2\pi m_2}{\Delta x_2}d},\quad m_2\in\mathbb{Z}. \tag{B.1}$$

One can remark that, for $m_2=0$, $D_\phi=1\ \forall d$, which means that no grid-to-grid dephasing occurs, even if $d\neq 0$. Therefore, whenever a sampling rate reduction or an interpolation is carried out, only the already frequency-shifted contents (i.e. all aliased modes) will suffer from such grid-to-grid dephasing.

References

[1] C. K. W. Tam, Computational aeroacoustics: An overview of computational challenges and applications, Journal of Computational Fluid Dynamics 18 (6) (2004) 247–567.
[2] S. E. Sherer, J. N. Scott, High-order compact finite-difference methods on general overset grids, Journal of Computational Physics 210 (2) (2005) 459–496.
[3] S. Redonnet, G. Cunha, An advanced hybrid method for the acoustic prediction, Advances in Engineering Software 88 (2015) 30–52.

https://doi.org/10.4208/cicp.060515.161115b Published online by Cambridge University Press

[4] S. Redonnet, Simulation de la propagation acoustique en presence d'ecoulements quelconques et de structures solides, par resolution numerique des equations d'Euler, Ph.D. thesis, Universite Bordeaux I, Bordeaux (Oct. 2001).
[5] S. Redonnet, D. Lockard, D. Khorrami, M. Choudhari, The non reflective interface: an innovative forcing technique for computational acoustics hybrid methods, International Journal for Numerical Methods in Fluids 81 (1) (2016) 22–44.
[6] E. Manoha, C. Herrero, P. Sagaut, S. Redonnet, Numerical prediction of airfoil aerodynamic noise, AIAA Paper 2002-2573.
[7] M. Terracol, E. Manoha, C. Herrero, E. Labourasse, S. Redonnet, P. Sagaut, Hybrid methods for airframe noise numerical prediction, Theoretical and Computational Fluid Dynamics 19 (3) (2005) 197–227.
[8] G. Desquesnes, M. Terracol, E. Manoha, P. Sagaut, On the use of high order overlapping grid method for coupling in CFD/CAA, Journal of Computational Physics 220 (1) (2006) 355–382.
[9] C. K. W. Tam, K. A. Kurbatskii, Multi-size-mesh multi-time-step dispersion-relation-preserving scheme for multiple-scales aeroacoustics problems, International Journal of Computational Fluid Dynamics 17 (2) (2003) 119–132.
[10] C. K. W. Tam, K. A. Kurbatskii, An optimized extrapolation and interpolation method for computational aeroacoustics, AIAA Paper 2001-0282.
[11] N. Pellers, A. L. Duc, F. Tremblay, M. Manhart, High-order stable interpolations for immersed boundary methods, International Journal for Numerical Methods in Fluids 52 (11) (2006) 1175–1193.
[12] D. Desvigne, O. Mardsen, C. Bogey, C. Bailly, Development of noncentered wavenumber-based optimized interpolation schemes with amplification control for overlapping grids, SIAM Journal of Scientific Computing 32 (4) (2010) 2074–2098.
[13] R. W. Schafer, L. R. Rabiner, A digital signal processing approach to interpolation, Proceedings of the IEEE 61 (6) (1973) 692–702.
[14] G. Cunha, S. Redonnet, On the signal degradation induced by the interpolation and the sampling rate reduction in aeroacoustics hybrid methods, International Journal for Numerical Methods in Fluids (DOI: 10.1002/fld.3693) 71 (7) (2013) 910–929.
[15] J. P. Boyd, Chebyshev and Fourier Spectral Methods, Springer-Verlag, 1989.
[16] P. Schmid, An Introduction to Computational Fluid Dynamics, John Wiley and Sons Inc., 2007.
[17] G. Cunha, S. Redonnet, Development of optimized interpolation schemes with spurious modes minimization, International Journal for Numerical Methods in Fluids 80 (2016) 140–158.
[18] K. A. Kurbatskii, C. K. W. Tam, Cartesian boundary treatment of curved walls for high-order computational aeroacoustics schemes, AIAA Journal 35 (1) (1997) 133–140.

https://doi.org/10.4208/cicp.060515.161115b Published online by Cambridge University Press